

Design Optimization and CFD and Performance Analyses of Miniature Axial-Centrifugal Flow Pumps for Circulating Molten Lead

Mohamed S. El-Genk^{1*}, Timothy M. Schreiner¹ and Andrew S. Hahn²

¹Nuclear Engineering Department, The University of New Mexico, Albuquerque, New Mexico

²Sandia National Laboratories, Albuquerque, New Mexico

Abstract

For circulating molten lead in compact in-pile and ex-pile test loops at 773.15 K this work developed a multi-physics methodology to optimize the designs of miniature axial-centrifugal flow pumps with impeller blades diameters of 55.0, 60.0 and 66.8 mm for maximizing the pumping power, the pump efficiency, and the pressure head. Increasing the diameter of the optimized impeller blades and/or the shaft rotation speed from 1,500 to 3,000 RPM increases the pump characteristics and efficiency, but also increases the dissipated thermal power. The molten lead flow rate at the peak efficiency increases with increased impeller shaft rotation speed and /or the blades outer diameter. The performed CFD analysis shows that rounding the tips of the blades and/or decreasing their clearance from 1.5 to 2.0 mm limit the formation of the flow vortices and the pressure losses and increases the pump efficiency. Results also show that increasing the molten lead temperature from 673.15 to 873.13 K slightly decreases the pump pressure head and negligibly affects the pump efficiency. This work successfully demonstrated the use of additive manufacturing of an impeller design with 60.0 mm diameter blades.

Keywords: Miniature axial-centrifugal flow pumps • Molten lead reactors • In-pile test loop • Design optimization • Performance analysis.

Abbreviations

(ADS) Accelerator Driven System; (AFA) Alumina Forming Austenitic; (AFMP) Axial-Centrifugal Flow Mechanical Pump; (ALFRED) Advanced Lead Fast Reactor European Demonstrator; (ALIP) Annular Linear Induction Pump; (CFD) Computational Fluid Dynamics; (CLEAR) China Lead-Based Reactor; (DC-EMP) DC-Electromagnetic Magnetic Pump; (GLP) Gas-Lift Pumping; (LBE) Lead-Bismuth Eutectic; (ODS) Oxide Dispersion Strengthened; (Pb) Molten Lead; (SCH) Schedule; (SMR) Small Modular Reactor; (VTR) Versatile Test Reactor; (ΔP) Pump Net Pressure Head (Pa); (m) Liquid Flow Rate (kg/s); (η) Pump Efficiency (%); (ρ) Liquid Density (kg/m³).

Introduction

Alkali and heavy metal cooled advanced, Small Modular Reactors (SMRs) and micro nuclear reactors are being developed for generation of electricity and production thermal power for a wide range of applications. SMRs and micro reactors nominally generate ≤ 300 MW_e and 20 MW_e, respectively, can produce process and district heat in populated and industrial regions as well as for remote communities and island nations for many years without refueling [1-11]. The low vapor pressures of liquid sodium (Na) and the heavy metals of molten lead (Pb) and lead-bismuth eutectic (LBE) eliminate the need for a pressure vessel and operate slightly below atmospheric at high temperature for achieving plant thermal efficiencies more than 40%. They also have excellent thermal properties and relatively low pumping requirements [6-8,10,12-14].

An important part of the development of liquid metals cooled advanced

and small and micro reactors is identifying suitable structure and cladding materials that are compatible with liquid Na, Pb, and LBE at high temperatures from 700 K-1000 K [17-21]. Ongoing investigations include single effect laboratory tests, ex-pile tests at or near operation conditions in liquid metals circulating loops, and in-pile tests in fast spectrum test reactors [18-20,22-25] to support future commercial operation licensing effort.

While liquid sodium and NaK alloys have been shown to be compatible with many austenitic stainless steels, ferritic or martensitic steel alloys, and super alloy materials, molten lead and LBE corrode many traditional structural and nuclear fuel cladding alloys when operating at temperature >723 K [19-20,22,24-25]. Therefore, investigating materials' compatibility at prototypic temperatures and under irradiation is essential to the development of future advanced reactors cooled by heavy liquid metals. This is done using small in-pile experimental loops. Examples are the LBE cartridge test loop in the Russian BOR-60 reactor [26,27] and the Versatile Test Reactor (VTR) design in USA [28,29].

Miniature-axial centrifugal flow pumps have previously been developed and used for circulating alkali liquid metals and heavy liquid metals in experimental test facilities, and for Accelerator Driven Systems (ADS) and small nuclear power reactors [30-37]. Grindell [31] had investigated compact centrifugal pumps with a 305 mm diameter impeller and inlet and outlet were connected to 3" SCH40 and 2" SCH pipe, respectively, in test loops of circulating liquid NaK-56 and water. Kelly et al. [30] had developed a compact turbine-driven single-stage centrifugal pump with an impeller outer diameter of 185.4 mm for circulating liquid NaK-78 at 978 K, 681 m³/hr, and pressure head of 928.4 kPa at impeller shaft speed of 8,000 RPM.

***Address for Correspondence:** Mohamed S. El-Genk, Institute for Space and Nuclear Power Studies and Nuclear Engineering Department, the University of New Mexico, Albuquerque, New Mexico, Email: mgenk@unm.edu

Copyright: © 2022 Mohamed S. El-Genk, et al. This is an open-access article distributed under the terms of the Creative Commons Attribution License, which permits unrestricted use, distribution, and reproduction in any medium, provided the original author and source are credited.

Received: March 16, 2022; **Manuscript No:** jme-22-57686 **Editor assigned:** March 18, 2022; **Pre QC No:** jme-22-57686 (PQ) **Reviewed:** April 01, 2022; **QC No:** jme-22-57686 **Revised:** April 06, 2022; **Manuscript No:** jme-22-57686 (R) **Published:** April 13, 2022; **Doi:** 10.37421/jme.2022.11.591

Reemsnyder, et al. [32] investigated the performance and potential cavitation of impeller blades for an axial flow pump circulating liquid sodium at 1,089 K. The 127 mm diameter impeller designs were fabricated of 316 and 318 stainless steels and Rene 41 alloy with as fabricated tip clearance of 1.64 mm, to achieve a flow rate of 63.6 m³/hr at a shaft speed of 3,450 RPM. Centrifugal pump designs for circulating liquid sodium have been tested, as part of the Large-Scale Breeder Reactor program [33], in a water loop for investigating the effect of the impeller blades cavitation on the pump performance. Different impeller designs were investigated in the test loop at shaft speeds ranging from 1,000 to 2,600 RPM.

Mirelas, et al. [34] have developed a miniature mechanical pump design for circulating NaK-78 for cooling a space nuclear power system for planetary surface power. The pump design with a 1.0 mm tolerance between the impeller rotor and the shroud and a 3-vane centrifugal impeller were used to circulate 823 K liquid NaK at 4 kg/s and 29.2 kPa, at shaft speed of 1,750 RPM. Lvov, et al. [35] have investigated cavitation in a variable speed centrifugal pump for circulating molten lead in an experimental loop at 743 K-773 K, shaft speeds up to 1,200 RPM and flow velocities of 25 m/s-30 m/s. They reported no conventional lead vapor cavitation occurred during the experiments. They reported no signs of erosive wear were observed on the surfaces of the pump impeller blades [35]. The HELENA test facility at ENEA Brasimone research center employed a centrifugal mechanical pump to circulate liquid lead [36] at 673 K, 10 kg/s-40 kg/s and pump heads of 350 kPa-500 kPa. The pump was constructed of austenitic stainless steel and with a tantalum plated stainless steel impeller for corrosion resistance in molten lead. The results of a CFD analysis indicated that at the maximum flow condition in the test loop the impeller would experience molten lead flow velocities up to 30 m/s. Breznosov, et al. [37] have experimentally tested 27 different impeller designs of an axial flow mechanical pump for circulating molten lead in advanced nuclear reactors. With a 200 mm diameter impeller, the experiments investigated the effects of the blade angle and solidity, and the number of blades on the pump performance at 713 K-773 K and shaft rotation speeds of 600-1,100 RPM. Results determined that for a three bladed impeller with 22° blades the pressure head and efficiency were higher than for the impellers with four and eight blades.

Several researchers have performed CFD analysis to estimate the performance of mechanical pumps for circulating heavy liquid metals such as molten lead and LBE. Mangialardo, et al. [38] have used the ANSYS CFD code [39] to investigate jet pumps for circulating liquid lead at 673 K lead and a flow rate of 3,274 kg/s in the Advanced Lead Fast Reactor European Demonstrator (ALFRED) fast reactor [38]. They used experimental data for water jet pumps to validate the CFD results, which suggested that the used sizing criteria of the jet pumps for water cooled reactors are applicable to molten lead pumps. However, the flow velocity of molten lead exiting the nozzle at up to 18 m/s is a concern for potential corrosion of structural metal alloys [38].

Lu, et al. [40] have performed CFD analysis of a LBE mechanical pump design developed for the China Lead-based Reactor (CLEAR-I), an LBE-cooled accelerator driven system [41]. They investigated the effects of the guide vanes at the impeller exit on the pump performance. The pump with an impeller outer diameter of 177 mm circulated LBE at 90 m³/hr, 593 K and a shaft speed of 980 RPM. At low flow rates the vanes increased the pump pressure head by 18%, however, the pump design without guide vanes showed superior performance at higher flow rates because of decreased pressure losses. The guide vanes increased the torque fluctuations on the impeller and the amplitude of the pressure fluctuations with increased rotation speed.

Svoboda, et al. [42] have performed CD analyses to investigate the performance of axial flow mechanical pumps with impeller diameters of 353, 350, and 272 mm for circulating liquid metal coolants. They reported good agreement of the CFD analyses results with experimental values to within ±5%. Recently, Zhang, et al. [43] performed CFD analysis of a centrifugal flow pump design with an impeller diameter of 248.0 mm for use in a LBE

test loop at 350 m³/hr, a pressure head of 433.9 kPa and shaft rotation speed of 750 RPM. Results showed significant flow separation at the pump outlet and that the developed high and low velocity regions increased internal pressure losses.

Mechanical pumps for circulating heavy liquid metals in ex-pile and in-pile testing loops need to be much smaller than those investigated in the literature. Suitable pumps could have an overall diameter <100 mm, low thermal energy dissipation, simple design for assembly and disassembly, and good characteristics for a wide range of circulation rates. Existing miniature centrifugal pumps, such as those used for deep water wells at ambient temperatures, are bulky with multiple stages and provide relatively low flow discharge. As suitable alternative is a single impeller miniature pumps specially designed to provide axial-centrifugal flow of heavy liquid metals, which is the focus of the present work.

The objectives of the present work are: (a) to develop and implement a multi-physics design methodology of miniature axial-centrifugal flow single impeller pumps with blades diameters of 50.0, 60.0 and 66.8 mm for circulating molten lead at 773.15 K (500°C) in pile test loops; (b) optimize pump designs for maximizing pressure head, efficiency, and pumping power; and (c) investigate the effects of rounding the impeller's blades, and the blades diameter and clearance from shroud wall on the pump performance. A design optimization methodology is developed which links the commercial CAESES optimization engine for pump design, the CFD code STAR-CCM+ (Siemens PLM, 2019), and the Sandia National Laboratory's DAKOTA design analysis software [44,45].

Miniature Axial-Centrifugal Flow Pump Design

Figure 1 shows section views of the present miniature axial-centrifugal flow pump design with the impeller blades and flow guide vanes for directing molten Pb flow in an annular downcomer. The flowing liquid along the spiraling blades of the impeller is accelerated centrifugally before exiting radially and flowing downward in the annular downcomer. The pump impeller has 11 main and 11 splitter blades (Figure 1). The splitter blades smooth the flow through the impeller, minimize flow eddies at the impeller exit, and limit the backflow between the impeller and shroud. The clearance between the impeller blades and the surrounding shroud wall accommodates thermal expansion to avoid contact of the blades with the shroud wall. A smoothed guide directs the exiting radial flow into the downcomer. The fixed vanes in the downcomer reduce swirling turbulence and guide the flow. The flow guide above the impeller exit fits within a small clearance around the wheel and inhibits liquid flow into the upper plenum. Figure 2 shows the incorporated pump assembly into a small diameter experimental cartridge like that employed in the BOR-60 test reactor [26] and considered for in-pile testing in the Versatile Test Reactor in the US [27-28]. The molten lead exiting the pump impeller flows down through a concentric annular downcomer to a hemispherical lower plenum then reverses direction to flow through the heated test section (Figure 2). The shaft bearings may either be submerged into molten lead or mounted outside depending on the design of the loop, liquid temperature, and the length, rigidity, and rotation speed of the drive shaft. The cartridge in Figure 2 is sized to fit within a hexagonal flow shroud equal in diameter to the regular reactor fuel assemblies. The molten lead flow in the downcomer of the test loop is cooled by the VTR sodium coolant flowing along the outer wall of the test cartridge loop (Figure 2).

The developed multi-physics methodology is applied for optimizing the pump designs with a 60 mm diameter impeller blades for circulating molten lead at 1.0 kg/s and 773.5 K and for pump designs with impeller diameters of 55.0 mm and 66.8 mm for circulating molten lead at 14 kg/s. For three impeller diameters the performance characteristics are evaluated as functions of the impeller shaft rotation speed. In addition, the effect of varying the molten lead temperature on the performance of the optimized

pump design with 55.0 mm diameter impeller blades is evaluated.

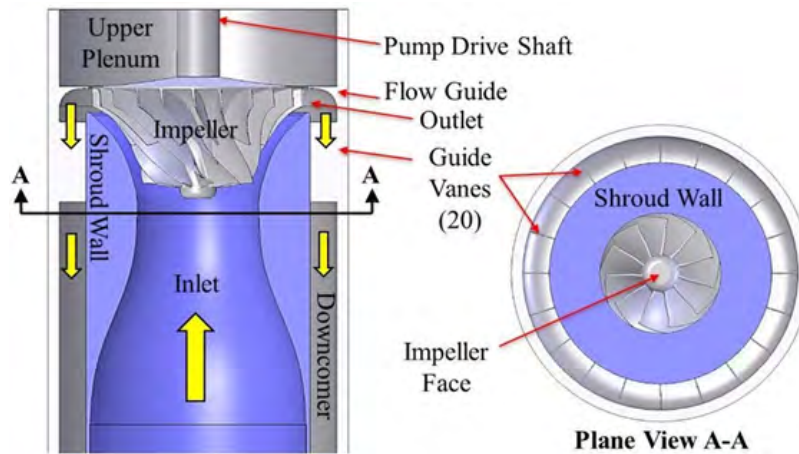


Figure 1. Section views of developed miniature axial-centrifugal flow pump design.

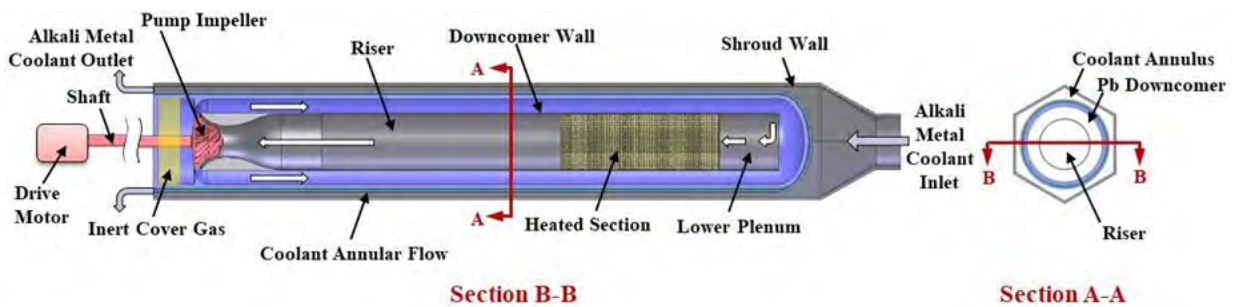


Figure 2. Cross-Sectional views of in-pile test cartridge with an axial-centrifugal flow pump.

Design Optimization Methodology

The developed miniature axial-centrifugal pump designs are optimized using a developed automated multi-physics methodology (Figure 3) that links the CAESES software for the pump design generation [46], the STAR-CCM+ commercial software for CFD performance analysis [44], and the open-source DAKOTA software for multivariable parameter optimization analysis using a genetic algorithm [45]. This methodology also investigated the effects of different geometric parameters on pump performance. These parameters are the shape and dimensions of the impeller blades, the hub, and the surrounding shroud wall. The CAESES software uses a matrix of equations to develop a solid geometry for the pump assembly for the desired blades diameter. The develop pump assembly is communicated to the STAR-CCM+ CFD software with the user specified fluid properties, inlet temperature, range of the flow rate, and the rotational speed of the impeller shaft. The CFD analysis simulates the liquid flow for the optimized blades of the impeller and calculates the pressure rise across the impeller and the induced momentum by the impeller as functions of the rotation speed. The CFD results return to the CAESES software to determine the pump characteristics, the impeller shaft power, the pumping power, and the pump efficiency. The calculated pump performance parameters are communicated to the DAKOTA along with the desired pump design optimization requirements such as the maximum pressure head, pumping power or pump efficiency. DAKOTA employs a multi-objective genetic algorithm that works on the principle of evolution; creating and testing generations of variables, which represent the 'genes' of the pump design.

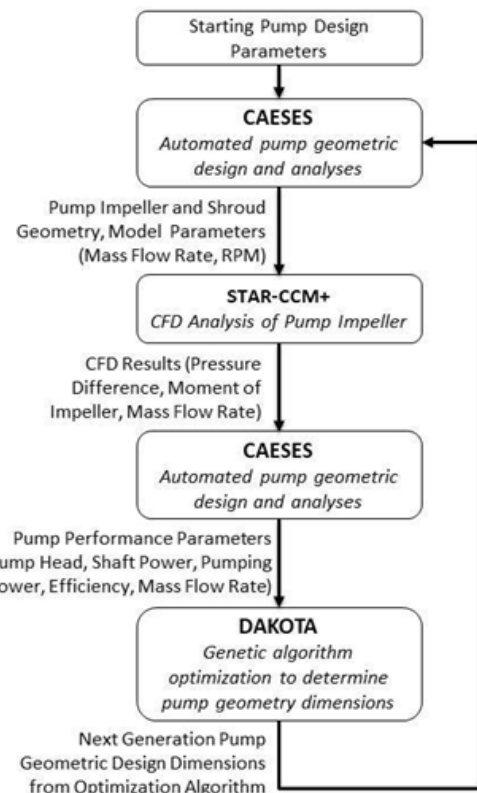


Figure 3. Multi-physics methodology of optimizing miniature axial-centrifugal-flow pumps.

The best performing combinations of the geometric parameters are selected and their 'genes' are mixed to produce the next generation of the pump design. The CAESES software uses the selected geometric design parameters by the DAKOTA's optimization algorithm to generate new solid design for CFD simulation to evaluate the performance of the new pump design. This iterative process continues until the multi-objective genetic algorithm in DAKOTA converges on an optimum pump design for the user specified performance requirements (Figure 3). This optimization methodology is used to optimize pump designs for the highest pumping power, pumping pressure head, and pump efficiency, as well to investigate the effects of changing the molten lead flow rates and the impeller diameter and shaft rotation speed, on the performance of the optimized pump designs.

Validation CFD simulation methodology

The implemented STAR-CCM+ simulation methodology is validated using experimental data of Beznosov, et al. [37] for a molten lead axial flow pump with a 4-blade impeller, rotor and hub diameter of 200 mm and 80 mm, respectively, a pitch of 28°, and a blade solidity of 1.0 (insert in Figure 5). The clearance between the impeller blades and the flow channel wall in the test was not reported. However, an 18 mm clearance in the performed CFD analysis resulted in the best agreement with the reported experimental data (Figure 5). Figure 4 shows images of the pump solid geometry with the specified fluid inlet and exit conditions and the implemented numerical mesh grid in the CFD analyses of the present optimized miniature axial centrifugal pump designs. These analyses used the rotating geometry feature in the STAR-CCM+ CFD code version 13.06.012 [44] to calculate the performance characteristics as functions of the rotation speed of the impeller shaft. The boundary conditions in the performed analyses are constant liquid mass flow, uniform inlet liquid velocity, and atmospheric pressure of 101.325 kPa at the exit of the flow annulus (Figure 4a). The liquid is treated as incompressible, thus properties are functions of temperature. The properties of molten lead in the CFD analyses are based on suggested correlations [12]. The STAR-CCM+ simulations used the SST k- ω turbulence model and an implicit unsteady solver with a maximum of 150 inner iterations per timestep with a residual convergence limit of 5.0×10^{-5} . The timestep size is scaled inversely proportional to the rotation speed of the impeller shaft, so that the simulation time decreases as the shaft rotational speed increases [44]. For an impeller shaft rotation speed of 1,500 RPM the major timestep used in the CFD analysis is 3.33 ms and 1.67 ms for a rotation speed of 3,500 RPM.

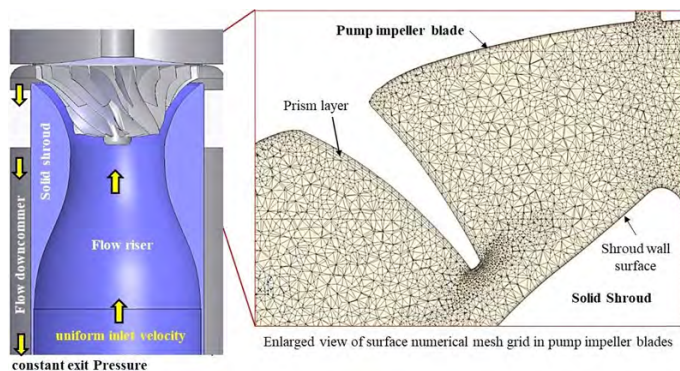


Figure 4. Molten lead inlet and exit conditions and the numerical mesh grid in the impeller for the performed CFD simulation analysis of the present axial-centrifugal flow pump designs.

The performed CFD analyses were performed for pump shaft rotational speeds of 600, 700, 1,000, and 1,100 RPM and a molten lead flow rate of 165 m³/h. Figure 5 plots the reported experimentally measured values of the pump pressure head versus those calculated in the present CFD analysis. The CFD analysis values of the pump head are in good agreement with the reported experimental to within $\pm 10\%$, confirming the suitability the implemented CFD analysis approach for investigating the performance

characteristics of the present axial-centrifugal flow pump designs for circulating molten Pb (Figures 1 and 4)

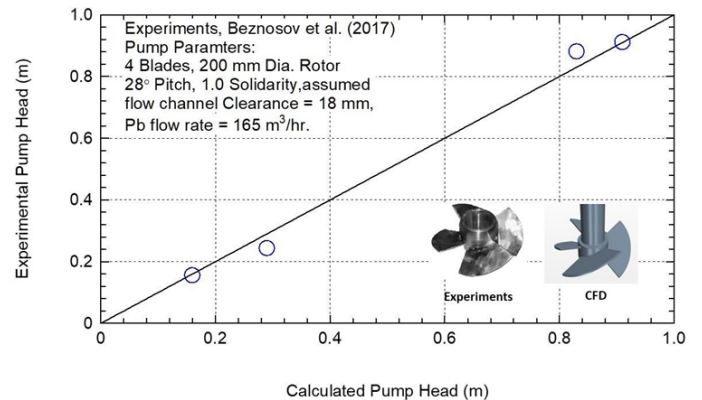


Figure 5. Comparisons of the present CFD results to the experimental data by Beznosov et al. [37].

Numerical meshing

The performed CFD analysis of the present pump design employed the tetrahedral volume mesher of the STAR-CCM+ code to generate the numerical mesh grid in the fluid regions (Figure 4). The enlarged section of the implemented numerical mesh grid in Figure 4 shows the higher densities of the numerical mesh cells near the edges and tip of the impeller blades. The mesher generates four parallel prismatic layers of a total thickness of 100 microns at the fluid-solid interfaces and an exponential growth factor of 1.3 for increasing the mesh cell size with distance from the fluid-solid interfaces. The smallest and the largest surface mesh cell size is set at 10 and 400 microns, respectively. The CFD analysis varied the smallest size of the surface tetrahedral mesh generated on the solid geometry to investigate the effect of refining the numerical mesh grid on the calculated pump performance.

The CFD analysis results presented in Figure 6 are for the optimized pump design (Figure 1) for maximizing pumping power with a 60 mm outer diameter impeller blades for molten Pb flow rates of 1.0 kg/s and 15 kg/s at 773.15 K. The results in Figure 6a at 1.0 kg/s show little change in the CFD analysis predictions with refining the numerical mesh grid. However, the results in Figure 6b at molten lead flow of 15 kg/s show a gradual decrease in the predicted pumping pressure head with decreased smallest cell size in the numerical mesh grid to 10 microns. Further refinements of the numerical mesh grid negligibly changes the calculated pump heads in the CFD analysis. Therefore, subsequent analysis performed to quantify the performance of the present pump designs used numerical mesh grids with 10 microns smallest surface mesh cell size.

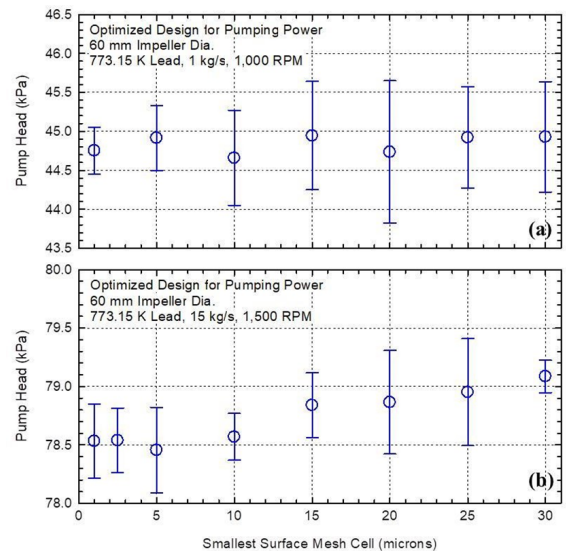


Figure 6. Effect of changing refining numerical mesh grid on pressure

heads for two pump designs.

Performance Results of Optimized Pump Designs

This section presents the calculated performance results of the optimized pump designs using the developed multi-physics methodology described above and presented in Figure 3. The first pump design is optimized for 1.0 kg/s molten lead flow with impeller blades diameter of 60.0 mm, and shaft

rotation speed of 1,500 RPM (Table 1). For this design, Figure 7 presents photographs of the 3-D printed pump impeller using additive manufacturing. The pump designs with impeller blades diameters of 55.0 and 66.8 mm and rotation speed of 1,500 RPM are optimized for a molten lead flow of 14 kg/. The 55.0 mm diameter impeller fits within a standard 2-inch SCH pipe, and the large diameter of 66.8 mm fits within a 2.5-inch SCH pipe. Other investigations include the effects on the pump characteristics of the choices of the optimization parameter in the DAKOTA software (Figure 3), rounding of the edges of the impeller blades, changing the clearance between the impeller and shroud wall, and molten lead temperature. The ranges of the



Figure 7. A 3-D printed plastic impeller of developed design of a miniature axial-centrifugal flow pump with 60 mm impeller blades diameter.

Table 1. Design parameters of optimized pump designs for molten Pb at 773.15 K.

Optimized Designs	Low Flow	High Flow
Optimization Parameter	Max. Pumping power, Max. Pump head, Max. Efficiency	Max. pumping power
Rotation Speed (RPM)	1,500	1,500
Molten Pb Flow Rate, <i>m</i> (kg/s)	1.0	14

Table 2. Performance parameters of optimized miniature axial-centrifugal flow pump designs.

Impeller Dia. (mm)	Pb Flow rate, <i>m</i> (kg/s)	Pb Temperature (K)	Rotation Speed (RPM)	Blade Edges	Shroud Clearance (mm)
60.0	0.0 to 30 kg/s	773.15	1,500, 2,500, 3,000	Sharp	2.0
55.0	0.0 to 30 kg/s	673.15, 773.15, 873.15	1,500, 2,500, 3,000	Sharp, Rounded	1.5 and 2.0
66.8	0.0 to 30 kg/s	773.15 K	1,500, 2,500, 3,000	Sharp, Rounded	1.5 and 2.0

parameters used are listed in Table 2.

Optimized pump impeller blades for circulating molten Pb flow at 1.0 kg/s

The developed miniature axial-centrifugal flow pump design methodology (Figure 3) is applied to optimizing the pump with 60 mm diameter impeller for molten lead flow of 1.0 kg/s at 773.15 K and impeller shaft speed of 1,500 RPM (Figure 8). This figure shows isometrical and cross-sectional views of the pump impeller. The impeller blades are optimized for maximizing the pumping power, the pump pressure head, and the pump efficiency. The optimized 60 mm diameter impeller has 11 primary and 11 splitter blades (Figure 8). It is incorporated into a pump assembly (Figure 1) with a circular tube diameter of 64 mm and a downcomer width of 10 mm. The calculated performance characteristics of the pumps with the three optimized impeller designs at shaft speed of 1,500 RPM and flow rates from 0 to 30 kg/s are presented in Figure 9.

The calculated pump characteristics for the three optimized impeller blades designs are compared in Figure 9a, and the corresponding pump efficiencies are compared in Figure 9b. The optimized impeller design for maximizing the pumping efficiency produces the highest pump characteristics and efficiency, followed by the those for maximizing pumping power. The characteristics and the efficiencies of the pump with the optimized impeller design for maximizing the pump pressure head are the lowest (Figure 9a). The developed pump pressure heads decrease monotonically with increased flow rate of molten lead from ~99.75, 96, and 86.9 kPa at zero flow rate to ~36.1, 28.25, and 24.8 kPa at a flow rate of 30 kg/s (Figure 9a). The pump efficiencies for all three impellers at a shaft speed of 1,500 RPM initially increase with increased flow rate to peak values then decrease with further increase in the molten lead flow rate. The peak efficiency for the pumps with optimized impellers for maximizing the pumping power and the pump head are ~28.7% and 27.8%, respectively, and occurs at the same molten lead flow rate of 13.8 kg/s. The peak efficiency for the pump with the optimized impeller design for maximizing efficiency is ~40.7% and occurs at

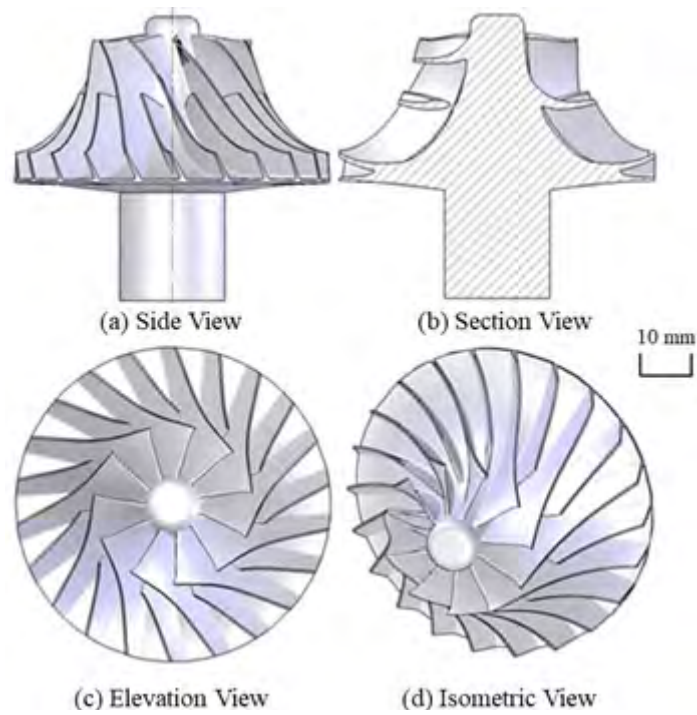


Figure 8. Isometric and cross-sectional views of the 60.0 mm diameter impeller for maximum pumping power at shaft speed of 1,50 RPM and for molten Pb at 1.0 kg/s and 773.15 K.

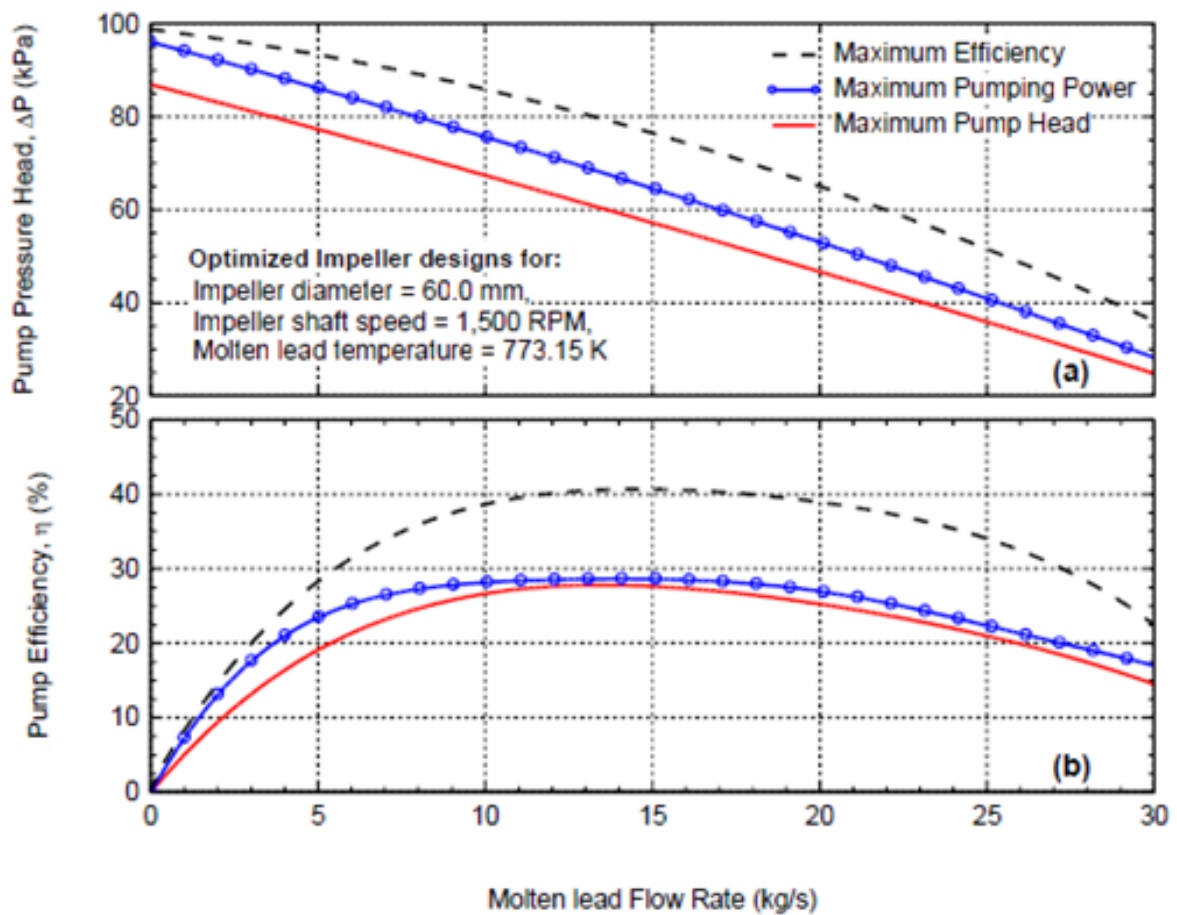


Figure 9. Calculated characteristics and efficiencies for pumps with optimized 60.0 mm diameter impellers for maximizing pumping power, pressure head, and pump efficiency.

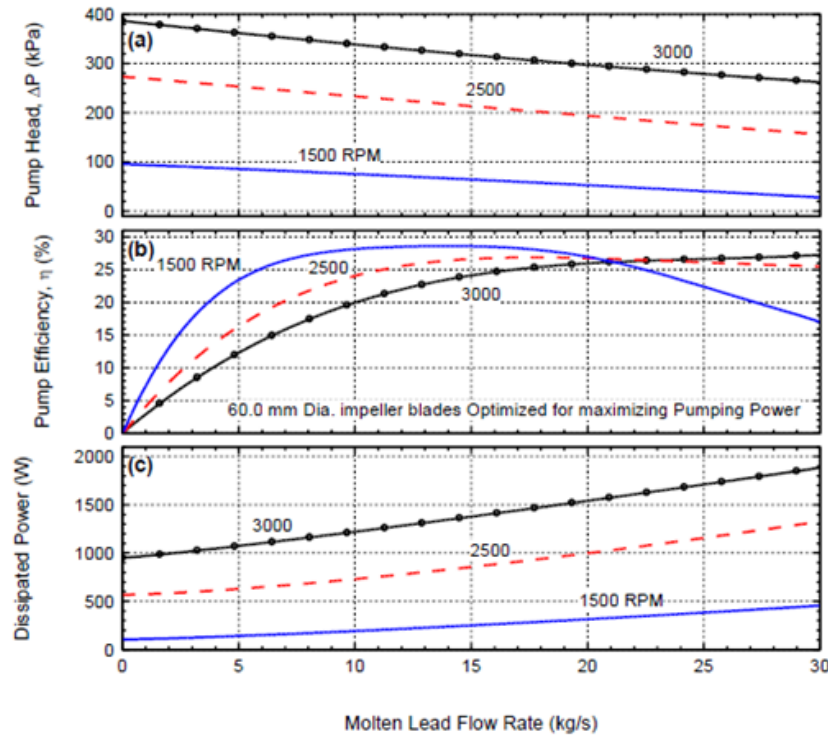


Figure 10. Comparison of generated pressure head, efficiency, and dissipated power for pump with optimized 60.0 mm diameter impeller blades for maximizing pumping power.

a molten lead flow rate of ~14.5 kg/s (Figure 9b).

Figure 10 presents results of the effect of changing the rotation speed of the impeller shaft on the pump characteristics (Figure 10a) and efficiency (Figure 10b) and the dissipated power into the flowing molten lead (Figure 10c). The dissipated power by viscous dissipation along the surfaces of impeller blades equals the difference between the impeller shaft mechanical power and the pumping power produced (Eq. 1a). Increasing the rotation speed of the impeller shaft markedly increases the pump pressure head (Figure 10a) along the entire range of the molten Pb flow rates investigated, 0 kg/s-30 kg/s. For all impeller rotation speeds investigated, the pump pressure head decreases linearly with increased flow rate. The produced pressure head at zero flow is the highest. At impeller shaft rotation speed of 1,500 RPM this pressure head is 96.1 kPa and increases to 273.5 kPa and 386.5 kPa with increased impeller shaft speed to 2,500 and 3,000 RPM, respectively (Figure 10a). At flow rates below ~19 kg/s, increasing the rotation speed of the pump impeller decreases the pump efficiency due to the increased viscous dissipation. Conversely at high flow rates, the pump efficiency increases with increased the rotation speed of the impeller shaft due to the increase in the pumping power produced (Figure 10b). The dissipated thermal power by the rotating impeller into the molten lead flow

increases both with increased flow rate and shaft rotation speed (Figure 10c). For the lowest speed of 1,500 RPM the dissipated thermal power at the highest flow rate of 30 kg/s is 452 W. This value increases to as much as 1.327 and 1.884 kW with increased rotation speed to 2,500 and 3,000 RPM, respectively.

Optimized pump impeller designs for molten Pb flow at 14.0 kg/s

This subsection presents the performance results for optimized impeller blades with diameters of 55.0 mm and 66.8 mm for circulating molten lead at 14 kg/s. The design optimization used the multi-physics methodology in Figure 3. The 55.00 mm diameter impeller's blades fit within 2-inch SCH standard size pipe with 2 mm clearance, and the 66.8 mm diameter impeller's blades fit within 2.5-inch SCH pipe also with 2 mm clearance. Figure 11 presents isometric and cross-sectional views of the 55.0 mm (Figure 11a) and 66.8 mm (Figure 11b) outer diameter impellers and Figure 12 shows views of the implemented numerical mesh grid for the 66.8 mm outer diameter impeller blades with sharp edges and with rounded edges and rounded shrouds wall (Figure 12). These impeller designs are optimized for maximizing pumping power at molten flow rate of 14.0 kg/s and impeller shaft speeds of 1,000, 1,500, and 3,000 RPM. Figures 13-20 present and

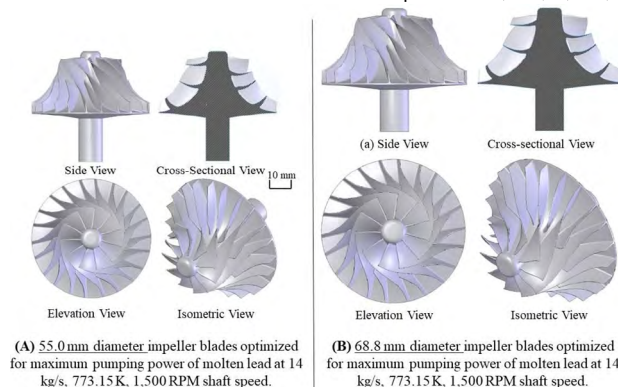


Figure 11. Isometric and cross-sectional views of pump impellers optimized for maximizing pumping power at shaft speed of 1,500 RPM.

compare the obtained performance results.

The optimized pump design with 66.8 mm diameter impeller blades with sharp edges (Figure 12a) generates a pressure head, $\Delta P=112.9$ kPa at molten lead flow rate of 15 kg/s and impeller shaft speed of 1,500 RPM (Figure 14b). The optimized designs with rounded blades edges decreases the flow pressure losses along the impeller blades (Figure 12b) and

increases the net pumping head at a molten lead flow rate of 15.0 kg/s by 7.6% to 121.5 KPs (Figure 14b). Increasing the rounding of the flow shroud wall (Figure 12b) also reduces the pressure losses for the exiting flow before entering the annular downcomer (Figures 1 and 4). The performed CFD analysis of the optimized pump designs with rounded impeller blades edges used a finer numerical mesh grid at the blades' tips, slightly increasing the total number of numerical mesh cells (Figures 12a and 12b).

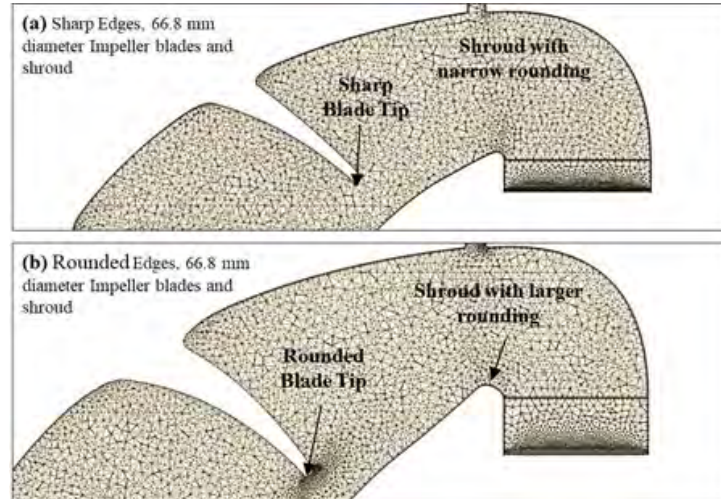


Figure 12. Implemented numerical mesh grid in CFD analysis for the pump with optimized 66.8 mm diameter impeller blades with: (a) sharp edges, and (b) rounded edges and flow shroud.

All performance results presented next are for optimized impeller designs with rounded blade edges and shroud (Figure 12).

The velocity fields presented in Figure 13 shows that decreasing the clearance from 2 mm to 1.5 mm increases the pumping pressure heads both at the low and high flow rates of molten lead of 1.0 and 15 kg/s. The larger clearance increases the reversed flow and flow mixing which increase pressure losses and decrease the net pump pressure head. At a molten lead flow rate of 1 kg/s, decreasing the clearance between the impeller

blades and the shroud wall from 1.5 to 2.0 mm increases the pumping head, ΔP , by 6.1% from 60.3 kPa to 64.0 kPa (Figures 13a and 13b). At the higher molten lead flow rate of 15.0 kg/s (Figures 13c and 13d) the reduced pressure losses within the impeller blades using the smaller clearance of 1.5 mm increase the net pump head by 20.1% from 63.1 kPa to 75.8 kPa. As the smaller 1.5 mm clearance provides improved pump performance, it is used in the subsequent analysis for the performance characterization of the pumps with optimized impeller blades for maximizing the pumping

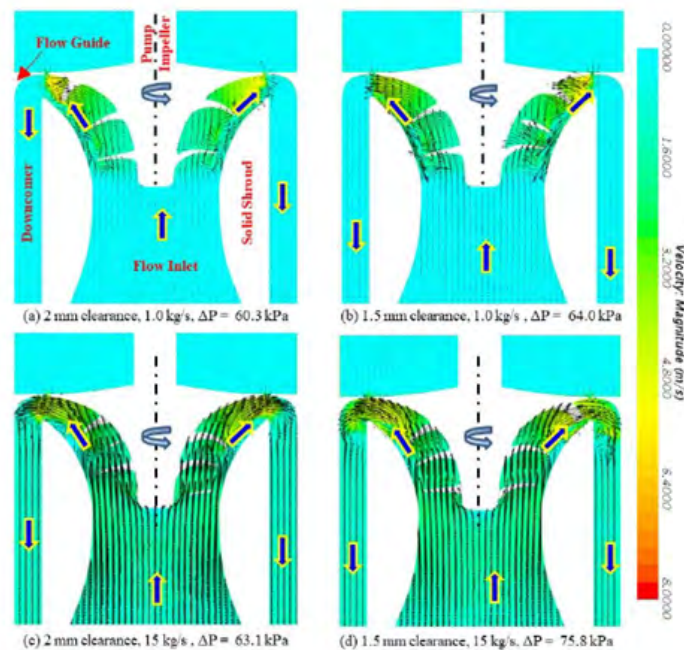


Figure 13. Effect of shroud clearance on velocity flow fields for a pump with optimized 55.0 mm diameter impeller blades for maximizing pumping power of molten Pb at 1.0 and 15.0 kg/s and shaft speed of 1,500 RPM.

power for molten lead flow rates from 0 kg/s-30 kg/s and impeller shaft rotation speeds of 1,500, 2,500, 3,000 RPM (Figures 14-20).

Figures 14-16 plot the calculated pumping head, efficiency, and dissipated power for the optimized pump designs with 55 mm and 66.8 mm diameter impeller blades. The presented results are for blades with rounded edges and a clearance of 1.5 mm between the tip of the impeller blades and the shroud wall. The CFD performance results show that the optimized pump design with 66.8 mm outer diameter impeller blades generates higher pumping

heads for molten lead flow at the same shaft rotation speed (Figures 14a and 14b). At zero flow, the static pressure head for the pump with 66.8 mm outer diameter impeller blades is ~62.5% higher than for the pump with the smaller 55.0 mm diameter blades (Figures 14a and 14b). At an impeller shaft rotation speed of 1,500 RPM, the pump with the 66.8 outer diameter impeller blades generates a static pressure head, $\Delta P=148.5$ kPa compared to 91.5 kPa for the pump with the smaller 55.0 mm diameter blades. At higher shaft rotation speeds of 2,500 and 3,000 RPM, the generated static pressure heads by the pump with the 66.8 mm diameter impeller blades are

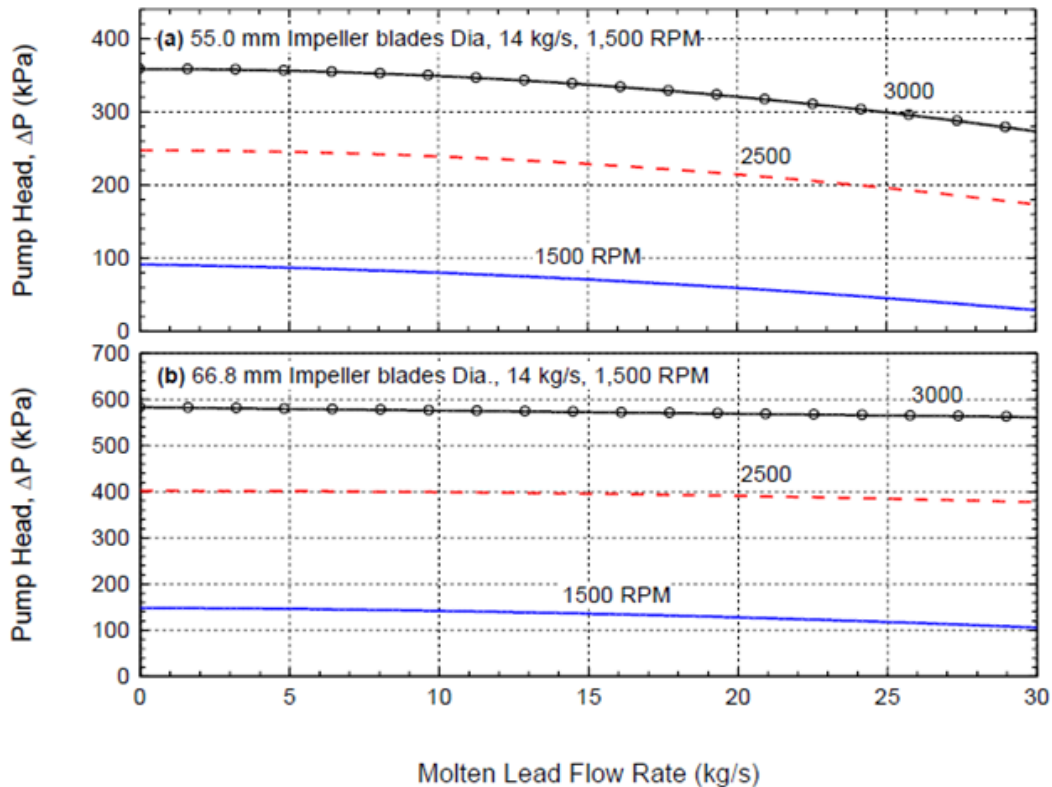


Figure 14. Comparison of performance characteristics of pumps with 55.0 mm and 66.8 mm outer diameter impeller blades optimized for maximum pumping power at 1,500 RPM and 14.0 kg/s.

401.8 and 582.8 kPa, respectively, compared to 247.3 and 358.4 kPa for the pump with 55.0 mm diameter blades (Figures 14a and 14b).

The characteristics for the pump with the 66.8 mm outer diameter impeller blades are not only much higher but also decrease less with increased flow rate of molten lead (Figure 14b), than for the pump with the 55.0 mm outer diameter impeller blades (Figure 14a). At an impeller shaft rotational speed of 1,500 RPM the generated pressure head for the optimized pump design with the 66.8 mm diameter impeller blades decreases 28.6% with increased molten lead flow from 0 to 30 kg/s. The decrease in the pumping pressure head gets smaller with increased rotation speed of the impeller shaft. At a shaft speed of 2,500 and 3,000 RPM the pumping pressure head at molten lead flow rates from 0 and 30 kg/s decreases by only 6.1% and 3.6%, respectively. In contrast, the pressure head generated by the optimized pump design with the smaller 55.0 mm diameter impeller blades at shaft rotation speeds of 1,500, 2,500, and 3,000 RPM with increased molten lead flow from 0 to 30 kg/s decreases 68.4%, 29.9%, and 23.8%, respectively. The pump with 55.0 mm and 66.8 mm outer diameter impeller blades optimized for maximum pumping power can achieve efficiencies of ~47%-49%, and the rate of heat dissipation to the molten lead slightly increases its temperature ~0.06 to 0.51 K at 15 kg/s because of relatively

high specific heat capacity of molten lead at 773.15 K (~145.1 kJ/kg. K) (Figures 15a and 15b) [12]. At the same shaft rotation speeds, the peak efficiencies for the pump with 66.8 mm outer diameter impeller blades occur at higher molten lead flow rates than for the pump with the smaller 55.0 mm diameter impeller blades. At an impeller shaft rotational speed of 1,500 RPM a peak efficiency of 47.4% for the pump with 55.0 mm outer diameter impeller blades occurs at a molten lead flow rate 10.1 kg/s, compared to 49.52% for the pump with the larger 66.8 mm outer diameter blades at a molten lead flow rate of 14.1 kg/s (Figures 15a and 15b). For a shaft rotation speed of 2,500 the peak efficiencies of the pumps with 55.0 mm and 66.8 mm diameter blades increase slightly to 47.8% at 15.2 kg/s, and to 49.7% at 22.5 kg/s, respectively (Figures 15a and 15b).

The dissipated thermal power by the pump to the flowing molten lead increases monotonically with increased flow rate and /or increased shaft rotation speed (Figure 15) and is significantly higher for the 66.8 mm outer diameter impeller blades (Figure 16b). For a shaft rotation speed of 1,500 RPM, the dissipated thermal power by the optimized pump design with the 55.0 mm diameter impeller blades increase from 57.6 W at zero flow to as much as 333.3 W at 30 kg/s (Figure 16a). The corresponding dissipated power for the pump with the larger 66.8 mm diameter impeller blades is

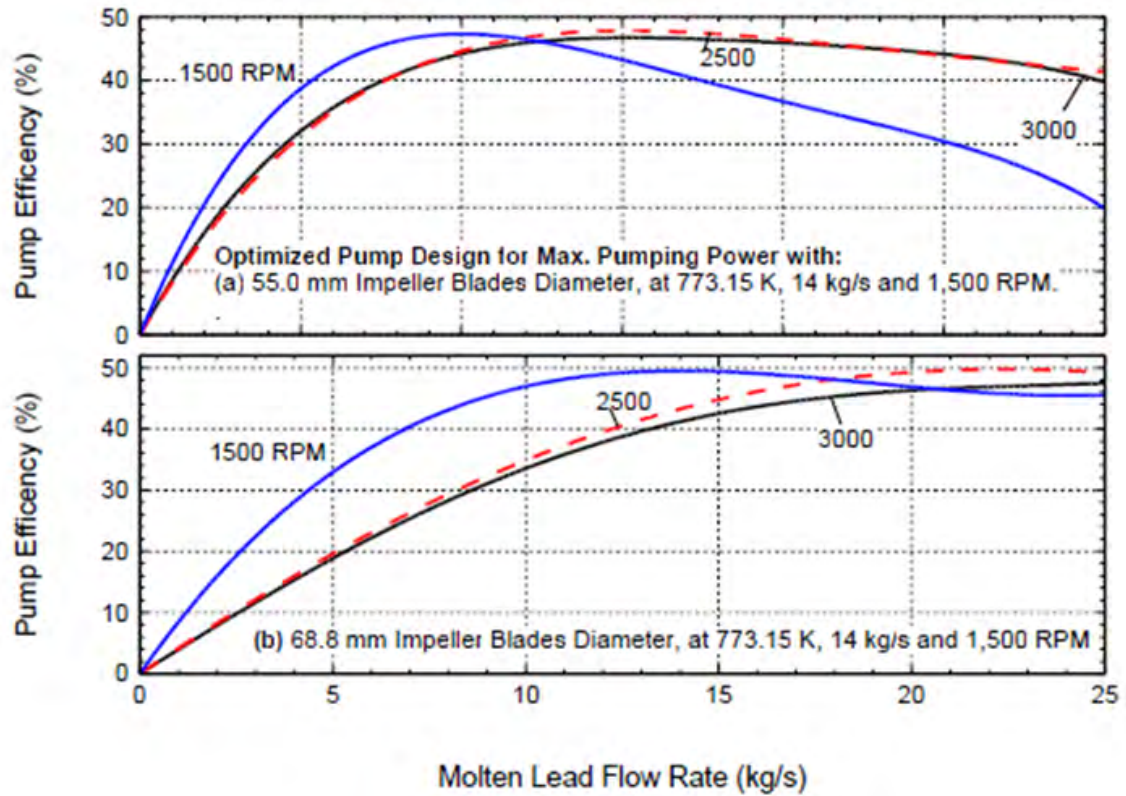


Figure 15. Comparison of the calculated efficiencies for the optimized pump designs with outer diameter blades of 55.0 mm and 66.8 mm for maximum pumping power.

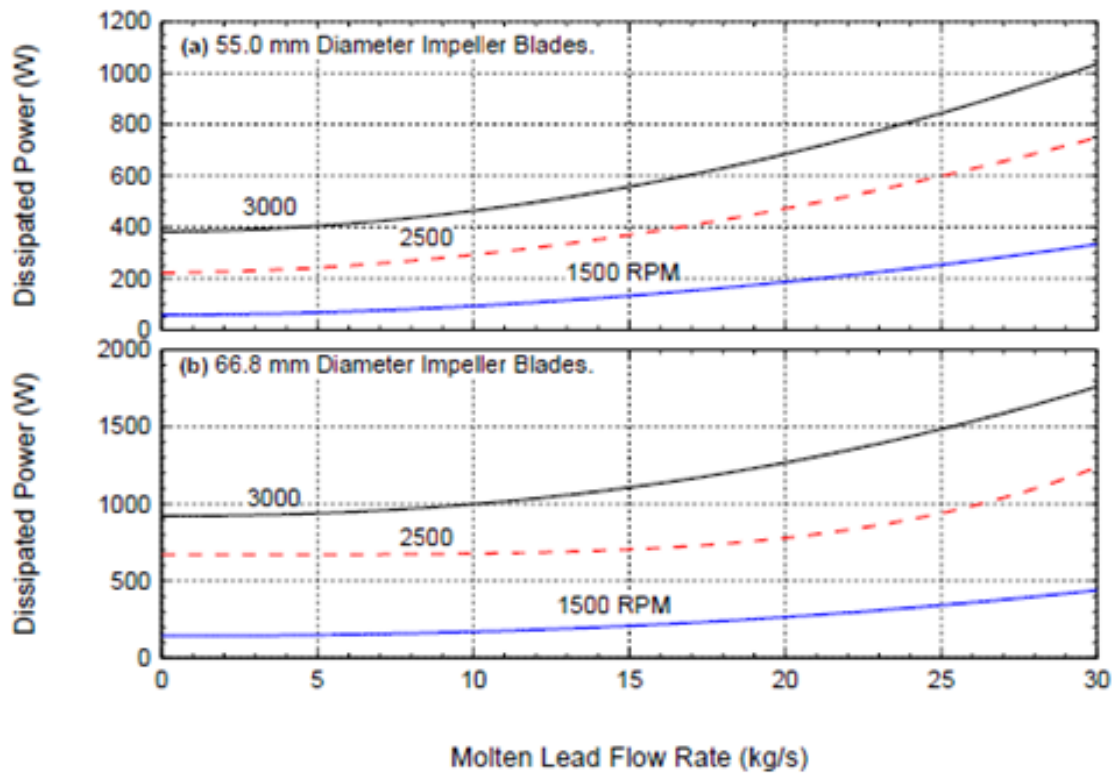


Figure 16. Comparison of dissipated power for pump designs optimized for pumping power with 55.0 mm and 66.8 mm outer diameter impeller blades.

143.0 W at zero flow rate (a 148% increase) and 439.4 W at 30 kg/s (a 31.8% increase), respectively.

At higher impeller shaft speeds of 2,500 and 3,000 RPM the dissipated thermal powers by the pump with impeller blades diameter of 66.8 mm are 201%, and 241% of those for the pump with smaller impeller blades diameter of 55.0 mm. The increase in the dissipated power between the 66.8 mm and 55.0 mm pump designs at 1,500, 2,500, and 3,000 RPM, respectively, at zero flow rate is much larger than the corresponding 62.5% increase in the pumping head. The pump design with 55.0 mm diameter impeller blades optimized for maximum pumping power has higher efficiencies and hence lower thermal power dissipation at lower flow rates. However, the results are reversed at high flow rates (Figures 15a and 15b). For a flow rate of 30 kg/s the pumping pressure head with the 66.8 mm diameter blades is 266%, 117%, and 206% that for the pump with the smaller 55.0 mm diameter blades at impeller shaft speeds of 1,500, 2,500, and 3,000 RPM, respectively. These increases in the pumping pressure head far exceed the corresponding increases in the dissipated power of 32%, 65%, and 70%, respectively. The results suggest that for applications requiring lower lead flow rates the pump design with 55.0 mm outer diameter impeller blades offers more efficient performance. On the other hand, the pump design with large 66.8 mm outer diameter impeller blades would be preferable for

higher flow rates applications.

The performed CFD analyses of the optimized pump designs calculate the molten lead flow velocity and pressure fields (Figures 17 and 18). The displayed images in these figures are for the optimized pump designs for maximum pumping power and with rounded blade edges and clearance of 1.5 mm. Figure 17 presented images of the calculated flow velocity field of the pump designs with impeller outer diameter blades of 55.0 and 66.8 mm, molten lead flow rate of 5 kg/s and impeller shaft rotation speeds of 1,500 and 2,500 RPM. Figure 18 presents images of the calculated pressure fields for the same conditions as in Figure 17. The white regions in these figures indicate the solid hardware of the impeller and its shaft, the walls of the flow shroud that reduces the cross-sectional area of the molten lead flow approaching the pump impeller, and the guides of the flow exiting the impeller blades to flow into the downcomer of the pump assembly. The velocity vectors in Figures 17a-17d show turbulent flow eddies in the flowing molten lead passing along the surface of the impeller blades. These eddies are produced due as the flow passing up along the impeller blades interacts with the limited back flow occurring in the space between the impeller blades and the shroud wall. The turbulent eddies and the local reversed flow effectively increase both the pressure losses and the dissipated thermal power and decrease the net pumping head and the

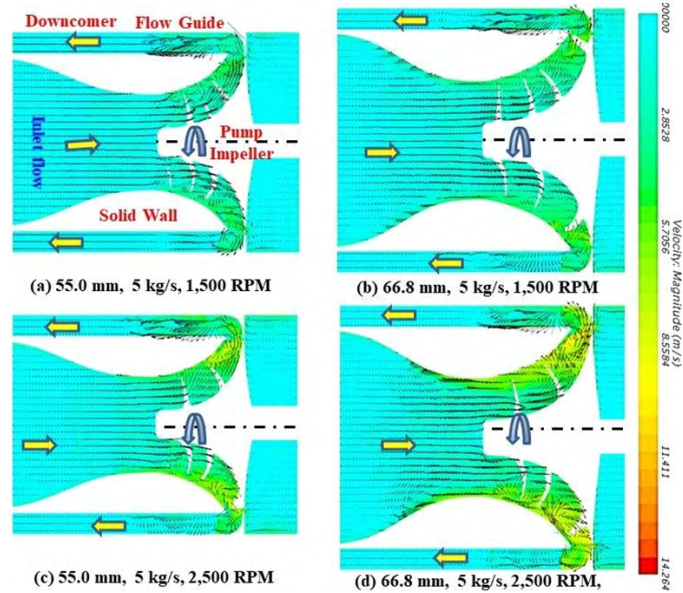


Figure 17. CFD images of velocity fields for optimized pump designs with 55.0 mm and 66.8 mm diameter impeller blades for molten Pb flow rate at 5 kg/s at 771.15 K.

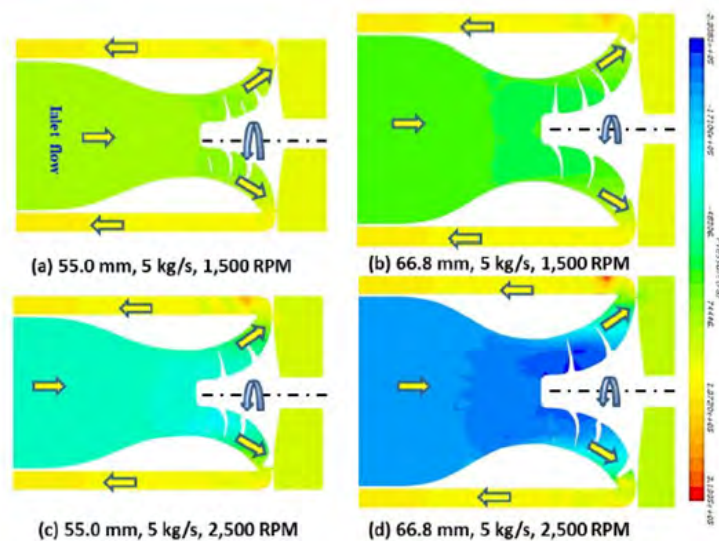


Figure 18. CFD images of calculated pressure fields for optimized pump designs with 55.0 mm and 66.8 mm outer diameter impeller blades.

pump efficiency (Figures 5 and 16). The intensity of the generated turbulent eddies at shaft rotation speed of 2,500 RPM (Figures 17a and 17b) are stronger than those at the lower speed of 1,500 RPM (Figures 17c and 17d).

The molten lead exiting the impeller blades is directed to flow through the downcomer with the aid of flow guides (Figure 1). The curved flow guides help reduce the intensity of the turbulent eddies in the flow, which help decrease the pressure losses. The installed longitudinal guide vanes in the downcomer (Figure 1) help straighten the flow in the annular downcomer (Figures 17a-17d). The velocity fields in Figure 17 show that the visible eddies cease as the guide vanes ensure a smooth down flow within the downcomer. The pressure field images in Figures 18a-18d show small local high-pressure regions where the flow exiting the impeller blades impinges

onto the outer wall of the downcomer.

In addition to the pump performance characteristics, the CFD analyses determine the maximum velocity for the flowing molten liquid metal along the surface and at the tips of the impeller blades (Figure 19). These velocities strongly influence the rates of corrosion and erosion along the surface of the metallic impeller by the flowing molten lead [19-20,22]. The rate of these processes increase as the molten lead flow velocity at the solid surface and tips of the impeller blades increases. They increase with increased rotation speed of the impeller blades and/or the diameter of the blades (Figure 19). The images in Figure 19 are for impeller shaft rotation speeds of 1,500 and 2,500 RPM and molten lead flow rate of 5 kg/s, same as in Figures 17 and 18.

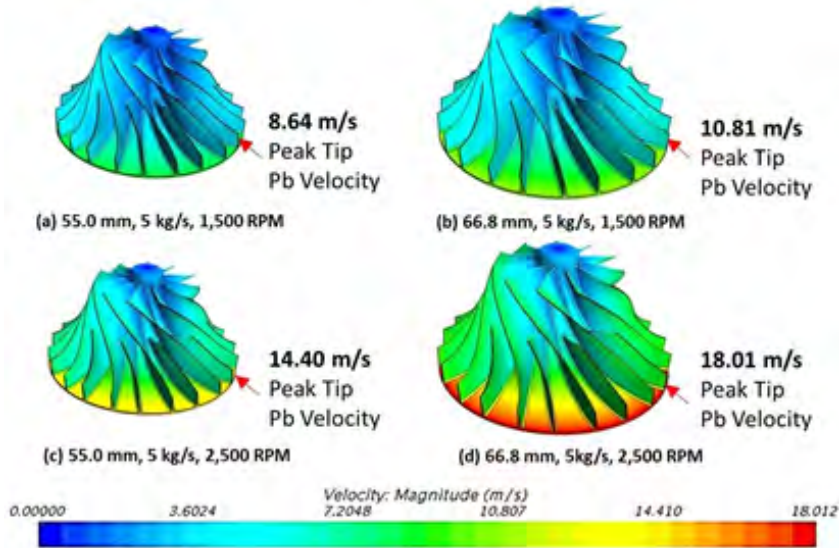


Figure 19. Velocities fields along the surface and at tip of impeller blades at shaft rotation speeds of 1,500 and 2,500 RPM, and molten Pb flow at 5 and 15 kg/s and 773.15 K.

The isometric views of the impeller blades show the colored coded surface of the impeller commensurate with the magnitudes of the molten lead flow velocities. The lowest velocity occurs at the stagnation point at the tip of the impeller hub facing the inlet flow (Figure 19). This figure shows that for the optimized 55.0 mm outer diameter impeller blades, the peak velocity at the tip increases from 8.6 m/s at a shaft rotation speed of 1,500 RPM to 14.4 m/s at a rotation speed of 2,500 RPM (Figures 19a and 19c). For the larger 66.8 mm outer diameter impeller blades, the peak velocity along the tips of the impeller blades increases from 10.8 m/s at a shaft rotation speed of 1,500 RPM to 18.0 m/s at 2,500 RPM (Figures 19b and 19d). At these velocities the corrosion rates of the metallic blades at 773.15 K should be sufficiently low to use austenitic 316 stainless steel for the impeller, blades, and the shroud wall. However, at higher temperatures the corrosion rate of 316 stainless steel would increase to exclude it from consideration and instead consider metallic alloys that are void of nickel such FeCrAl ODS steel and 9CrODS and 12CrODS steels [24-25].

Effect of working fluid temperature on pump performance

The previous results presented above are for molten lead flow at a temperature of 773.15 K. Changing the molten lead temperature will change its physical properties (Table 3) and hence the pressure losses and the net pump pressure head. The performed analyses investigated the effect of the working fluid temperature on the performance of the pump with the optimized 55.0 mm diameter impeller blades for maximizing the pumping power. The calculated performance characteristics of the pump for molten lead temperatures of 673.15 K and 873.15 K and shaft rotation speed of 2,500 RPM are presented in Figures 20a-20c. Increasing the molten lead temperature decreases its density and its dynamic viscosity ([12] and Table 3). The supplied pump pressure head is nearly the same for molten lead temperatures of 673.15 K and 773.15 K and slightly lower

at the higher temperature of 873.15 K (Figure 20a). At such temperature the lower density molten lead is more difficult to pump, reducing the net pumping pressure head slightly by <6 kPa compared to those at the lower temperatures (Figure 20a).

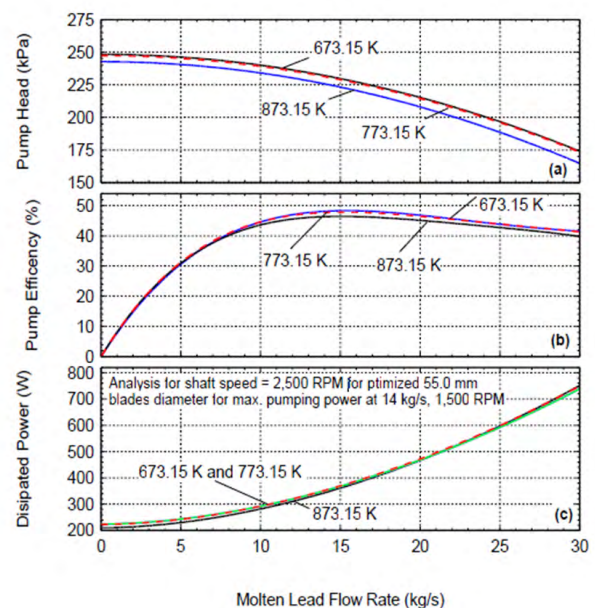


Figure 20. Effect of temperature on the pressure head, efficiency, and the dissipated power at shaft rotation speed of 2,500 RPM.

The results in Figure 20b show that the calculated pump efficiency is practically identical for molten lead flow rates <7 kg/s and at molten lead between 673.15 K and 873.15 K. At higher flow rates the pump efficiency is slightly higher for molten lead temperature of 673.15 K, followed by those at 773.15 K, and 873.15 K. The lower pumping head for circulating molten lead at 873.15 K is because of the decrease in the liquid density, despite the

decrease in the dynamic viscosity (Figure 20a, Table 3). The difference in the dissipated power into the circulating molten lead is practically the same irrespective of its temperature but increases fast with increased molten lead flow rate (Figure 20b) which increases the dissipated power being highest. The results in Figure 20 confirms the small effect of increasing the molten lead temperature on the pump performance parameters, suggesting that

Table 3. Molten Pb Thermophysical properties at 673.15, 773.15, and 873.15 K (OECD 2015).

Lead Temperature	Liquid Density (kg/m ³)	Specific Heat Capacity, Cp (J/kg-K)	Dynamic Viscosity (Pa-s)	Thermal Conductivity (W/m-K)
673.15 K	10,579.7	146.7	2.227×10^{-3}	16.6
773.15 K	10,451.8	145.1	1.813×10^{-3}	17.7
873.15 K	10,323.8	143.5	1.548×10^{-3}	18.8

the present axial-centrifugal flow pump designs optimized for circulating molten lead at 773.15 K would be applicable at different temperatures.

Discussion

A multi-physics design methodology is developed and applied to the design optimization and performance analysis of the miniature axial-centrifugal flow pumps for maximizing the pumping power, pump efficiency, or the pump pressure head. The developed design optimization methodology links the CAESSES software for the pump design generation, the STAR-CCM+ commercial software for CFD performance analysis, and the open-source DAKOTA program for multivariable parameter optimization analysis using a genetic algorithm. The optimized designs of miniature axial centrifugal flow pumps would be an attractive choice for in-pile and ex-pile test loops to support the development of advanced heavy liquid metals cooled nuclear reactors. Conducted analyses investigated the effects on the pump performance of increasing the outer diameter of the impeller blades from 55.0 mm to 66.8 mm, the shaft rotation speed from 1,500 to 3,000 RPM, the clearance between the edge of the blades and the shroud wall from 1.5 to 2.0 mm, and the molten lead temperature from 673.15 to 873.15 K. Additive manufacturing is successfully demonstrated of the optimized design with 60.00 mm diameter impeller blades for maximum pumping power.

The implemented CFD analysis methodology of the liquid lead flow through the axial-centrifugal flow pump is validated for simulating the performance of a molten lead axial flow pump used in the experiments of Beznosov et al. [37]. The calculated pump pressure heads agree with the reported experimental values to within $\pm 10\%$. This methodology is used in the present work to optimize the performance of the developed miniature axial-centrifugal flow pump designs for circulated molten lead in test loops.

Results show that increasing the impeller blades outer diameter and / or the shaft rotation speed increase the pump characteristics and efficiency and the dissipated thermal power. The flow rate at the peak efficiency increases with increased impeller shaft rotation speed and / or the impeller blades outer diameter. Increasing either the diameter of the optimized impeller blades or the shaft rotation speed increases the pump pressure head, the dissipated power, and the molten Pb flow rate at the peak efficiency. Rounding the tips of the impeller blades and/or decreasing their clearance from the shroud wall from 2.0 to 1.5 mm limit the formation of flow vortices, decreases pressure losses, and increases the pump efficiency. Increasing the molten lead temperature from 673.15 to 873.13 K slightly decreases the pumping pressure head and negligibly affects the pump efficiency. In addition to the pump characteristics and performance parameters, the CFD analysis provides detailed images of the velocity and pressure flow fields and of the induced vortices in the clearance between the blades and the shroud wall.

Conclusion

The optimized miniature pump designs with impeller blades diameters of 50.0, 60.0 and 66.8 mm could be fabricated using precision 3-D additive manufacturing and used for circulating heavy liquid metals such as molten lead, LBE, and Pb-Li alloys, as well as alkali liquid metals in fast spectrum micro and small modular nuclear reactors and both in-pile and ex-pile test loops. Other potential applications of these pumps include accelerator driven neutron sources using liquid lead or LBE targets, or Pb-Li blanket test loops for nuclear fusion experiments. Such pumps could also be used in a wide range of industrial applications such as circulating molten aluminum in metal casting plants, deep water wells, and liquid metals cooled microreactors. This work successfully demonstrated using additive manufacturing of an optimized impeller design with 60.0 mm diameter blades.

Acknowledgments

This work is partially funded by Battelle Energy Alliance, LLC Award No. 145662 to the University of New Mexico, and the University of New Mexico's Institute for Space and Nuclear Power Studies. We are grateful for having access to the resources of the High-Performance Computing Center at Idaho National Laboratory, which is supported by the Office of Nuclear Energy of the U.S. Department of Energy and the Nuclear Science User Facilities under Contract No. DE-AC07-05ID14517. We are also grateful to the UNM Center for Advanced Research Computing, supported in part by the National Science Foundation, for providing access to its high-performance computing capabilities. We are also grateful to Friendship Systems, Germany, <https://www.caeses.com/>, for the use of the CAESSES software, free of charge, to optimize of the developed pump designs.

References

1. Vujic, J, Bergmann RM, Skoda R and Miletic M, et al. "Small modular reactors: Simpler, safer, cheaper". *Energy* (2012) 45: 288–295
2. IAEA. "Advance in small modular reactor technology developments-A supplement to the iaea advanced reactors information system (ARIS)". *Inter Atom Ener Agen* (2016)
3. Hahn, D, Kim Y, Lee CB and Kim S, et al. "Conceptual design of the sodium-cooled fast reactor". *Nucl Eng & Tech* (2007) 39:193-206
4. Triplett, BS, Loewen EP and Dooies BJ."PRISM: A competitive small modular sodium-cooled reactor". *Nucl Tech* (2012) 178: 186-200.
5. Peakman, A, Hodgson Z and Merk B. "Advanced micro-reactor concepts". *Prog Nucl Ener* (2018) 107: 61-70.
6. El-Genk, MS, Palomino LM and Schriener TM. "Low-enrichment and long-life scalable liquid metal cooled small modular reactor (SLIMM-1.2)". *J Nucl Eng & Des* (2017) 316: 163-185
7. El-Genk, MS and Palomino LM. "A walk-away safe, very small, long-life,

- modular (vsllim) reactor for portable and stationary power". *Ann Nucl Ener* (2019) 129: 181-198
8. Ferroni, P. "The westinghouse lead fast reactor". *Advan Nucl Pow Plan* (2019)
 9. Ferroni, P. "Demonstrating the natrium reactor and integrated energy system". *Ter Pow* (2021)
 10. Kasilov, VF, Dudolin AA and Krashennnikov SM. "Development of a thermal scheme for a cogeneration combined-cycle unit with an SVBR-100 reactor". *Therm Eng* (2017) 64: 97-103
 11. Li, WG. "Effects of viscosity of fluids on centrifugal pump performance and flow pattern in the impeller". *Inter J Heat and Fluid Flow* (2000) 21: 207-212.
 12. Fazio, C. "Handbook on lead-bismuth eutectic alloy and lead properties, materials compatibility, thermal-hydraulics, and technologies". *NUCLEUS* (2015)
 13. Gromov, BF. "Use of lead-bismuth coolant in nuclear reactors and accelerator-driven systems". *Nucl Eng & Des* (1997) 173: 207-217
 14. Sakamoto, Y, Garnier JC, Rouault J and Grandy C, et al. "Selection of sodium coolant for fast reactors in the US, France and Japan". *Nucl Eng & Des* (2013) 254:194-217
 15. Zrodnikov, AV, Chitaykin VI, Gromov BF and Grigoryv OG, et al. "Use of russian technology of ship reactors with lead-bismuth coolant in nuclear power". *Inter Nucl Info* (2000) 31: 127-155
 16. Pacio, J, Singer CS, Wetzel TH and Uhlig R, et al. "Thermodynamic evaluation of liquid metals as heat transfer fluids in concentrated solar power plants". *Appl Therm Eng* (2013) 60: 295-302
 17. Allen, TR, Sridharan K, Tan L and Windes WE, et al. "Materials challenges for generation iv nuclear energy systems". *Nucl Tech* (2008) 162: 342-357
 18. Cheon, JS, Lee CB, Lee BO and Raison JP, et al. "Sodium fast reactor evaluation: Core materials". *J Nucl Mat* (2009) 392: 324-330.
 19. Fazio, C, Benamati G, Martini C and Palombarini G, et al. "Compatibility tests on steels in molten lead and lead-bismuth". *J Nucl Mat* (2001) 296: 243-248
 20. Muller, G, Heinzl H, Konys J and Schumacher G, et al. "Results of steel corrosion tests in flowing liquid pb/bi at 420-600°C after 2000h." *J Nucl Mat* (2002) 301: 40
 21. Nikitina, AA, Ageev VS, Leont'eva-Smirnova MV and Mitrofanova NM, et al. "Advances in structural materials for fast-reactor cores." *Atom Ener* (2016) 119: 362-371.
 22. Zhang, J, Li N, Chen Y and Rusanov AE, et al. "Corrosion behaviors of US steels in flowing lead-bismuth eutectic (LBE)." *J Nucl Mat* (2005) 336: 1-10
 23. Dubuisson, P, de Carlan Y, Garat V and Blat M, et al. "ODS ferritic/martensitic alloys for Sodium Fast Reactor fuel pin cladding." *J Nucl Mat* (2012) 428: 6-12
 24. Navas, M and Hernandez R. "Compatibility of structural materials with lead and lead bismuth eutectic for CSP applications." *AIP* (2018) 2033
 25. Anderoglu, O, Marino A and Hosemann P. "Corrosion in Heavy Liquid Metals for Energy Systems." (2021) 73: 3998-3999.
 26. Orlov, V, Filiin A, Sila-Novitski and Pikalov A, et al. "The BOR-60 loop-channel design for testing the brest reactor fuel. in power reactors and sub-critical blanket systems with lead and lead-bismuth as coolant and/or target material." *IAEA* (2003)
 27. Balderrama, S, Sabharwall P and Wachs D. "Versatile test reactor for advanced reactor testing." *Transact Amer Nucl Soc* (2018) 119: 942-945
 28. Kim, SJ. "Development of conceptual lead cartridge design to perform irradiation experiments in VTR." *Nucl Sci & Eng* (2022)
 29. El-Genk, MS, Schriener TM, Hahn AS and Altamimi R, et al. "Design optimization and performance of pumping options for VTR extended length test assembly for lead coolant (ELTA-CL)-update." *ISNPS* (2020)
 30. Kelly, RW, Wood GM and Marman HV. "Development of a high temperature liquid metal turbopump." *J Eng Pow* (1963) 85: 99-106
 31. Grindell, AG. "Correlation of cavitation inception data for a centrifugal pump operating in water and in sodium potassium alloy (NaK)." *ORNL* (1965)
 32. Reemsnyder, DC, Cunnan WC and Weigel C. "Performance and cavitation damage of an axial-flow pump in 1500°F (1089 K) liquid sodium." *Lew Resea Cent* (1969)
 33. Baladi, JY and Nyilas CP. "The development of a cavitation free sodium pump for the breeder reactor." *West Res & Develop Cen* (1986)
 34. Mirelas, OR, Bradley DE and Godfroy T. "Design of a mechanical nak pump for fission space power." *Inter Ener Conver* (2011): 1-5
 35. Lvov, AV, Bokov PA, Shumilkov AI and Novozhilova OO, et al. "Experimental investigation of cavitation in the circulation pumps with lead and lead-bismuth coolants." *Nucl Eng* (2012)
 36. Di Piazza, I, Tarantino M, Agostini P and Gaggini P, et al. "Helena: A heavy liquid metal multi- purpose loop for thermal-hydraulics, corrosion and component test." *Nucl Eng* (2014)
 37. Breznosov, AV, Lvov AV, Bokov PA and Bovova TA, et al. "Experimental studies into the dependences of the axial lead coolant pump performance on the impeller cascade parameters." *Nucl Ene & Tech* (2017) 3: 141-144
 38. Mangialardo, A, Borreani W, Lomonaco G and Magugliani F, et al. "Numerical investigation on a jet pump evolving liquid lead for GEN-IV reactors." *Nucl Eng & Des* (2014) 280: 608-618
 39. ANSYS workbench user guide (2014)
 40. Lu, Y, Zhu R, Fu and Wang QX, et al. "Research on the structure design of the LBE reactor coolant pump in the lead base heap." *Nucl Eng & Tech* (2019) 51: 546-555
 41. Wu, Y, Bai Y and Song Y. "Conceptual design of China lead-based research reactor CLEAR-I." *Chin J Nucl Sci & Eng* (2014) 34: 201-208
 42. Svoboda, DG, Zharkovskii AA, Ivanov EA and Shchutskii SYu, et al. "High-efficiency axial pumps for reactor use." *Russ Eng Res* (2019) 39: 556:560
 43. Zhang, Y, Kang C, Zhu Y and Kim HB, et al. "Investigation on the performance and flow characteristics of a liquid lead-bismuth pump." *J Mech Sci & Tech* (2021) 35: 2939-2947
 44. "Simcenter STAR-CCM+." Siemens (2019)
 45. Swiller, LP, Eldred MS and Adams BM. "Dakota: Bridging advanced scalable uncertainty quantification algorithms with production deployment." *Hand Uncert Quantif* (2017): 1651-1693"
 46. "Friendship Systems." CAESES (2020)

How to cite this article: El-Genk, Mohamed S, Timothy M. Schreiner and Andrew S. Hahn.. "Design Optimization and CFD and Performance Analyses of Miniature Axial-Centrifugal Flow Pumps for Circulating Molten Lead." *J Material Sci Eng* 11 (2022); 1-14